Available online at www.sciencedirect.com

SciVerse ScienceDirect

Ceramics International 39 (2013) 4673–4678

CERAMICS INTERNATIONAL

www.elsevier.com/locate/ceramint

Short communication

Lithium-ion insertion kinetics of Nb-doped $LiMn_2O_4$ positive-electrode material

Ting-Feng Yi[a,c,d,*], Long-Cheng Yin[b], Yong-Quan Ma[d], Hao-Yu Shen[c,d], Yan-Rong Zhu[a], Rong-Sun Zhu[a]

[a]School of Chemistry and Chemical Engineering, Anhui University of Technology, Maanshan, Anhui 243002, People's Republic of China
[b]Key Laboratory of New Carbon-based Functional and Super-hard Materials of Heilongjiang Province, Mudanjiang Normal College, Mudanjiang, Heilongjiang 157012, People's Republic of China
[c]Postdoctoral Research Station of Chemical Engineering & Technology, Harbin Institute of Technology, 150001 Harbin, People's Republic of China
[d]Chilwee Power Co., Ltd, Changxing, Zhejiang 313100, People's Republic of China

Received 7 October 2012; received in revised form 28 October 2012; accepted 28 October 2012
Available online 5 November 2012

Abstract

Nb-doped $LiMn_2O_4$ materials were synthesized by a solid state process, and the structure and kinetic performance were characterized by TG-DTA, XRD, SEM, CV, and EIS. TG-DTA shows that the decomposition reaction has almost completed and all reactions have finished at the temperature of 590 °C. XRD indicates that the all samples are in accordance with the standard spinel $LiMn_2O_4$. However, it can be found that little Nb^{5+} ions do not completely substitute Mn^{3+} ions of $LiMn_{2-1.667x}Nb_xO_4$ ($x=0.02$, 0.03, 0.04). SEM reveals that the average particle size of all samples is about 1 μm. CV exhibits that the improved reversibility and dynamic behaviors of $LiMn_2O_4$ can be attributed to the Nb doping. EIS demonstrates that Nb doping decreases the charge transfer resistance of $LiMn_2O_4$, and then reduces the cell impedance. Nb doping results in lower electrode polarization and a high lithium ion diffusion coefficient, and can effectively improve the kinetic performance of $LiMn_2O_4$.

Keywords: Positive-electrode material; $LiMn_2O_4$; Nb doping; Kinetic property

1. Introduction

Lithium-ion batteries have received intense attention as the power source in hybrid electric vehicles (HEVs), plug-in hybrid electric vehicles (PHEVs), and full electric vehicles (EVs) among the currently available energy storage technologies due to the high energy density [1,2]. Spinel $LiMn_2O_4$ has received a great deal of attention as the most promising positive-electrode material for lithium-ion battery because of its low cost, high safety and lower toxicity compared with the layered oxides $LiCoO_2$ and $LiNiO_2$ [2]. However, the Jahn–Teller distortion associated with the high spin Mn^{3+} results in a huge volume change and severe capacity fade at the deeply discharged state [3,4]. Hence, we hope that Mn^{3+} ion can be decreased in our synthesized product. As a result, we design the composition of $LiMn_{2-1.667x}Nb_xO_4$($x=0$, 0.01, 0.02, 0.03, and 0.04). They also can be further denoted as $LiMn_1^{4+}Mn_{1-1.667x}^{3+}Nb_xO_4$ ($x=0$, 0.01, 0.02, 0.03, and 0.04). The electrochemical performance of $LiMn_2O_4$ has been improved by doping with metal ions (such as Ni^{2+}, Al^{3+}, Cr^{3+}, Co^{3+}, etc.) [5–8] or non-metal ions (F^-) [9] in Li, Mn or O sites, or reducing the particle size [10]. It has been reported that Nb doping can be considered as an effective way to improve the electrochemical performance of spinel $LiMn_{1.5}Ni_{0.5}O_4$ and $Li_3V_2(PO_4)_3$ positive-electrode material [11,12]. Some soft chemistry routes, such as sol–gel [13], emulsion [14], combustion method [15], hydrothermal [16], microwave-induced combustion method [17], etc., have also been proposed. These methods lead to homogeneous spinel materials with

*Corresponding author at: School of Chemistry and Chemical Engineering, Anhui University of Technology, Maanshan, Anhui 243002, People's Republic of China. Tel.: +86 555 2311807; fax: +86 555 2311822.
E-mail address: tfyihit@163.com (T.-F. Yi).

0272-8842/$ - see front matter © 2012 Elsevier Ltd and Techna Group S.r.l. All rights reserved.
http://dx.doi.org/10.1016/j.ceramint.2012.10.256

smaller particle size. However, these methods also suffered from use of expensive reagents and process complexity. From a commercial viewpoint, the solid-state synthesis of LMn_2O_4 material exhibits a potential commercial application due to the simple synthesis route and low synthesis cost. The rate determining step in the electrodes of lithium ion batteries is supposed to be a solid state diffusion. The chemical diffusion coefficient describes the transport property of mobile species under a concentration gradient. Hence, it is important to investigate the lithium-ion transport processes for intercalation materials, and then study chemical diffusion coefficient of lithium ion to understand the intrinsic kinetic property of the electrode material [18]. The chemical diffusion coefficients of inserted ions in solid electrodes can be estimated by galvanostatic intermittent titration technique (GITT) [19], potentiostatic intermittent titration technique (PITT) [20], capacity intermittent titration technique (CITT) [21], and electrochemical impedance spectroscopy (EIS) [22]. EIS is considered as a very powerful technology to determine the rate of individual electrode kinetic steps because it can also be obtained under more equilibrium conditions compared with other methods. In addition, it has been reported that the cathode-side impedance, especially the charge transfer resistance (R_{ct}), is the main contributor to the cell impedance [23]. Therefore, the stability of interface can be reflected during the cycle of positive-electrode materials by comparing with the change of charge transfer resistance. To our knowledge, the kinetic performance of Nb-doped $LiMn_2O_4$ was not reported. In the present paper, $LiMn_{2-1.667x}Nb_xO_4$(x=0, 0.01, 0.02, 0.03, and 0.04) is successfully synthesized by a solid-state method, and the structure and kinetic properties are evaluated.

2. Experimental

2.1. Material preparation

Spinel $LiMn_{2-1.667x}Nb_xO_4$(x=0, 0.01, 0.02, 0.03, and 0.04) samples were synthesized by a solid-state reaction process. Stoichiometric Li_2CO_3 (AR, 99.0%), MnO_2 (GR, 98.0%), and Nb_2O_5 (AR, 99.9%) were mixed and ground in a mortar. Then the mixtures were calcined in air to 850 °C in an alumina crucible at a rate of 10 °C min^{-1}. The calcination at 850 °C was held for 18 h followed by a natural cooling to room temperature so that the final products were obtained.

2.2. Material characterization

Differential thermal analysis (DTA) and thermogravimetry (TG) measurements were performed in air from room temperature to 800 °C with a Henjiu Chare Tianping-1/2 thermal analysis system (Beijing, China) under a scanning rate of 10 °C min^{-1}. The crystalline structures of the samples were characterized by X-ray diffraction (XRD). The morphology and particle size were characterized by scanning electron microscopy (SEM). Cyclic voltammograms (CV) of the cells were measured at room temperature on a CHI 852C electrochemical workstation (China) in the voltage range from 3.3 to 4.5 V at the scanning rate of 0.2 mV s^{-1}. EIS measurements were carried out in two-electrode cells by using CHI 760D electrochemical workstation (China) with a $\pm$5 mV AC signal and a frequency range from 10^5 to 0.1 Hz. The positive-electrodes were adopted as the work electrode; the counter electrode and reference electrode were Li foil. Charge–discharge performance was characterized galvanostatically on Land 2000 T (China) tester at 0.2C rates between 3.3 and 4.5 V (vs. Li/Li^+).

2.3. Battery preparation

The electrochemical properties of the Nb-doped $LiMn_2O_4$ samples were measured in the CR2032 coin-type half-cells. Slurry was formed by mixing the active material (80%), acetylene black (10%), and binder (10 wt% polyvinylidene fluoride, dissolved in N-methyl-2-pyrrolidone). The slurry was coated onto the aluminum foil from which pellets of 14 mm in diameter were cut as

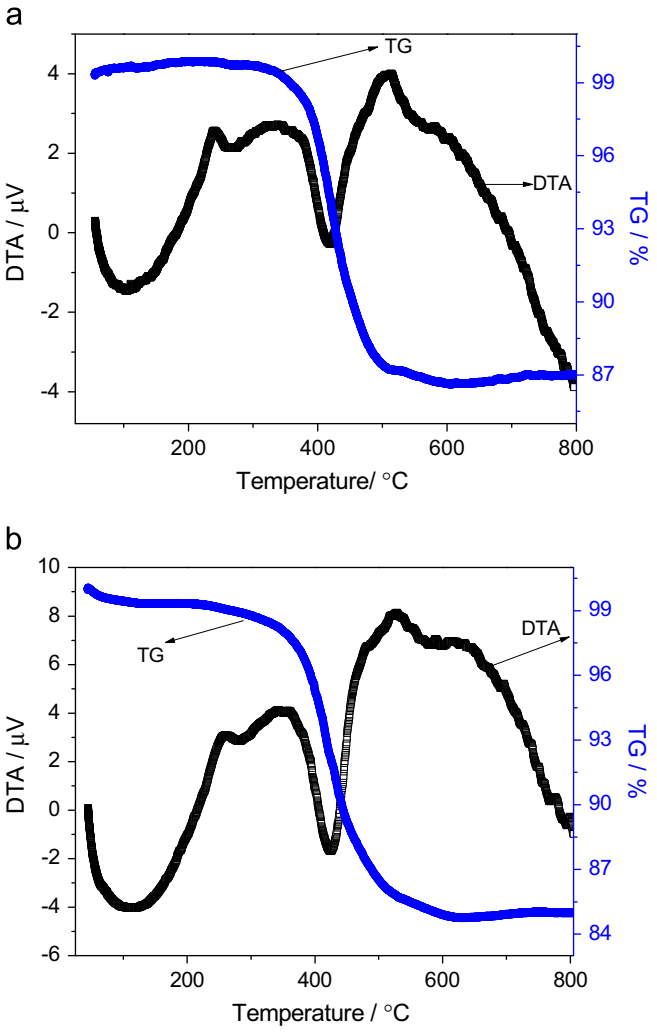

Fig. 1. TG-DTA curves for the thermal decomposition of the precursors of $LiMn_{2-1.667x}Nb_xO_4$: (a) x=0 and (b) x=0.01.

electrodes. The complete coin cell comprises a positive-electrode, a porous polypropylene membrane (Celgard 2300) as the separator and lithium foil anode. 1 M $LiPF_6$ dissolved in a mixture of ethylene carbonate and dimethyl carbonate (1:1 by volume) was used as the electrolyte.

3. Results and discussion

Fig. 1a and b shows the TG-DTA curves of $LiMn_{2-1.667x}Nb_xO_4$ (x=0, 0.01) obtained from the ternary precursors of Li_2CO_3, MnO_2 and Nb_2O_5. There are three temperature intervals where significant mass loss can be detected. The first one is the interval between room temperature and about 200 °C due to the removal of moisture and entrapped water [24]. In the second region (250–495 °C), two exothermic peaks observed are accompanied by noticeable weight loss in the TG curve. This can be ascribed to the decomposition of the inorganic constituents of the precursor followed by crystallization of the spinel phase. The obvious exothermic peak located at around 512 °C and a small exothermic peak located at around 590 °C in the DTA curves can be assigned to the phase-change reaction, the formation $LiMn_{2-1.667x}Nb_xO_4$ (x=0, 0.01), and the completion of crystallization reaction. It corresponds to the following reaction

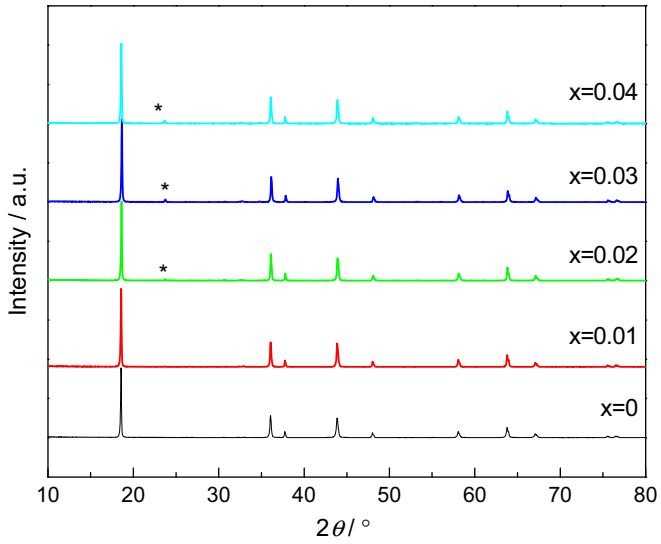

Fig. 2. XRD patterns of $LiMn_{2-1.667x}Nb_xO_4$ (x=0, 0.01, 0.02, 0.03, and 0.04) prepared by the solid state method.

$$Li_2CO_3 + 4MnO_2 \rightarrow 2LiMn_2O_4 + CO_2 + 0.5O_2 \quad (1)$$

$$Li_2CO_3 + 3.966MnO_2 + 0.01Nb_2O_5 \rightarrow 2LiMn_{1.983}Nb_{0.01}O_4 + CO_2 + 0.491O_2 \quad (2)$$

In the last region, the TG curve becomes flat and no sharp peaks can be observed in the DTA curve, indicating that no phase transformation occurs, and that any further heating only makes the structure of samples more perfect. Therefore, it is necessary to calcine the precursor mixture above 590 °C to obtain the well-crystallized $LiMn_{2-1.667x}Nb_xO_4$. In this study, thermal conversion into $LiMn_{2-1.667x}Nb_xO_4$ with subsequent crystalline growth was prepared by heat treatment at 850 °C for 18 h. Fig. 1a and b also indicates that the Nb doping does not change the reaction mechanism and the phase transition reaction.

Fig. 2 shows the X-ray diffraction patterns of $LiMn_{2-1.667x}Nb_xO_4$ (x=0, 0.01, 0.02, 0.03, and 0.04) samples prepared by

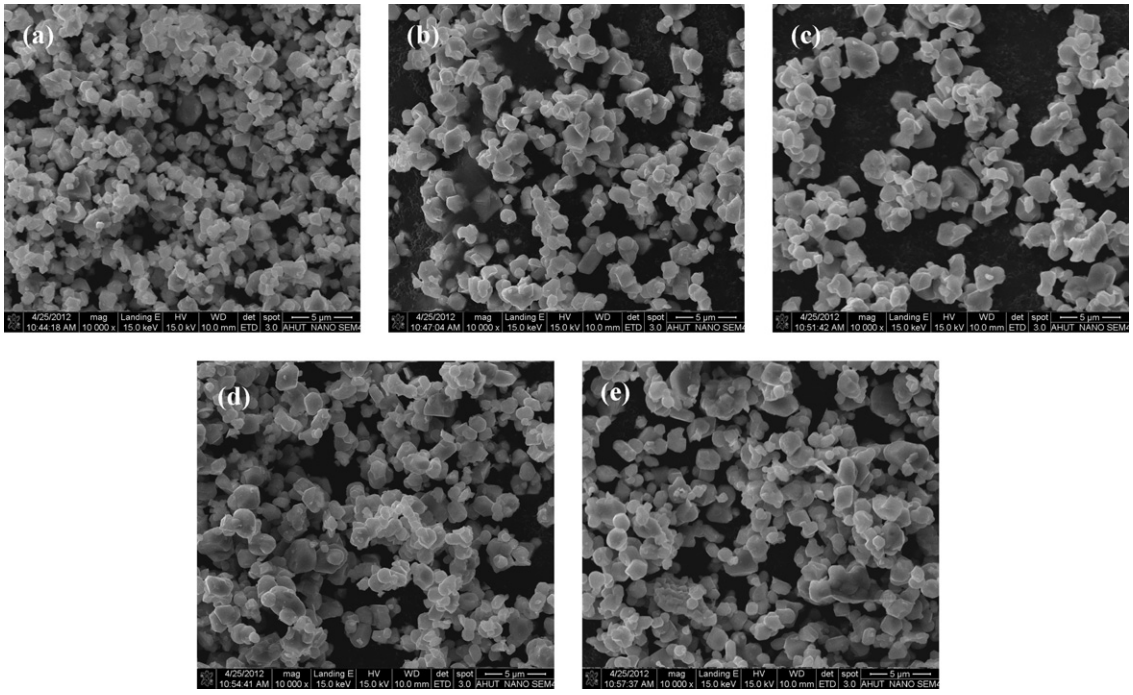

Fig. 3. SEM images of $LiMn_{2-1.667x}Nb_xO_4$: (a) x=0, (b) x=0.01, (c) x=0.02, (d) x=0.03 and (e) x=0.04.

the solid-state route. The diffraction peaks of the powders conform to JCPDS Card no. 89-0118, indicating that the synthesized powders are in accordance with the standard spinel $LiMn_2O_4$. However, there is some impurity in the patterns of $LiMn_{2-1.667x}Nb_xO_4$ (x=0.02, 0.03, and 0.04) samples, indicating that little Nb^{5+} ions do not completely substitute Mn^{3+} ions. Hence, it is important that a proper Nb doping level should be optimized to achieve a pure spinel structure.

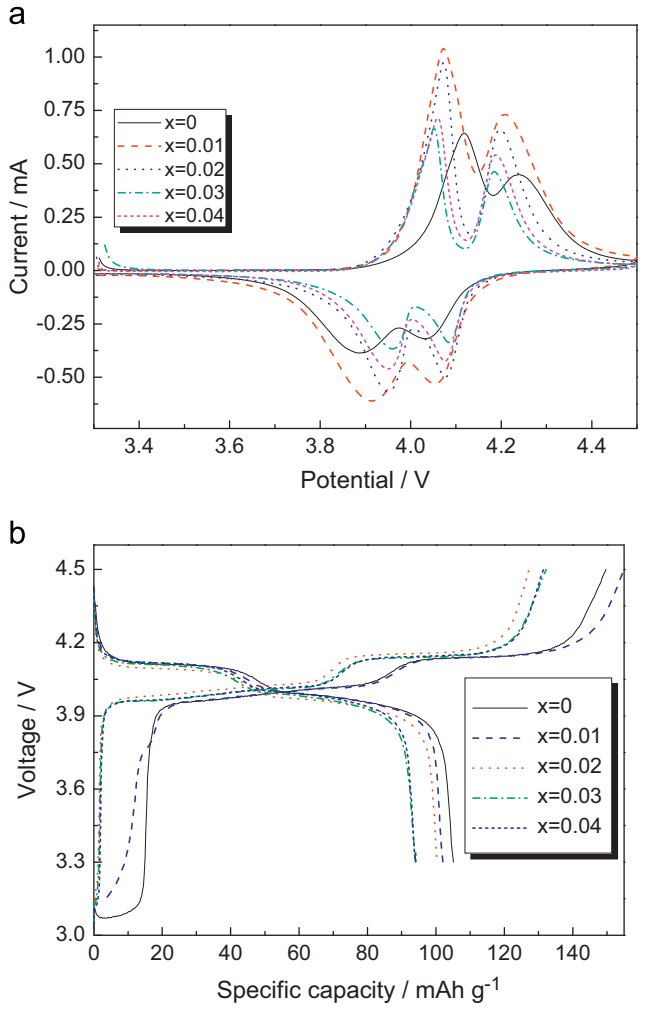

Fig. 4. Electrochemical performance of Li/ $LiMn_{2-1.667x}Nb_xO_4$ (x=0, 0.01, 0.02, 0.03, and 0.04) half cells: (a) cyclic voltammogram at a voltage sweep of 0.2 mV s^{-1} and (b) initial charge–discharge curves at 0.2 C.

The SEM images of $LiMn_{2-1.667x}Nb_xO_4$ (x=0, 0.01, 0.02, 0.03, and 0.04) samples are shown in Fig. 3. It can be seen that sample powders are uniform with a small grain size and the average particle size of all samples is about 1 μm. However, there is a great extent of agglomeration of particles in the $LiMn_2O_4$ samples. The results indicate that the Nb doping can restrain the agglomeration of solid powders during high temperature calculations. An increased porosity of Nb-doped $LiMn_2O_4$ may increase the electrode–electrolyte contact area and facilitate the lithium ions transportation, and then improve the electrochemical performance.

Cyclic voltammograms and initial charge–discharge curves for $LiMn_{2-1.667x}Nb_xO_4$ (x=0, 0.01, 0.02, 0.03, and 0.04) spinel are presented in Fig. 4, and their values of the CV peak are listed in Table 1. The redox peaks of all electrodes show well-defined splitting, which indicates that the powders exhibit good crystallinity. There are two anodic and cathodic peaks for $LiMn_2O_4$ and the substituted spinel. These two pairs of

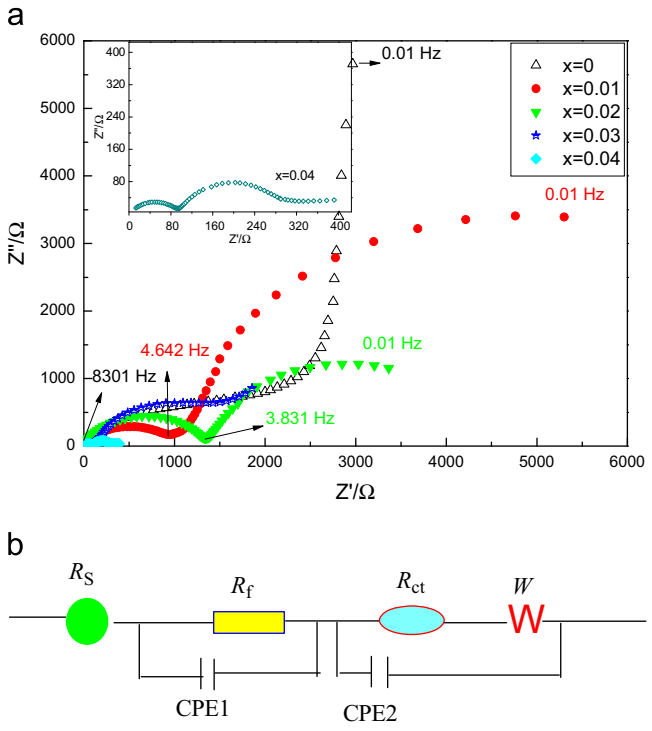

Fig. 5. (a) Nyquist plots and (b) equivalent circuit of $LiMn_{2-1.667x}Nb_xO_4$ (x=0, 0.01, 0.02, 0.03, and 0.04) electrodes.

Table 1
Values of the CV peaks for $LiMn_{2-1.667x}Nb_xO_4$ (x=0, 0.01, 0.02, 0.03, and 0.04) samples.

Samples	φ_{pa1} (V)	φ_{pc1} (V)	$\Delta\varphi_{p1}$ (mV)	φ_{pa2} (V)	φ_{pc2} (V)	$\Delta\varphi_{p2}$ (mV)
$LiMn_2O_4$	4.118	3.890	228	4.238	4.037	201
$LiMn_{1.983}Nb_{0.01}O_4$	4.702	3.915	157	4.205	4.055	150
$LiMn_{1.967}Nb_{0.02}O_4$	4.073	3.953	120	4.197	4.078	119
$LiMn_{1.95}Nb_{0.03}O_4$	4.055	3.963	92	4.185	4.085	100
$LiMn_{1.933}Nb_{0.04}O_4$	4.057	3.961	96	4.187	4.073	114

redox peaks correspond to a two-step reversible intercalation reaction [25], in which lithium ions occupy two different tetragonal 8a sites in spinel $Li_xMn_2O_4$ ($x<1$). The first oxidation and reduction peaks at 3.9–4.0 V corresponding to the second charge–discharge plateaus (Fig.4b) can be attributed to the removal of lithium ions from half of the tetrahedral sites in which Li–Li interactions occur. The second oxidation and reduction peaks corresponding to the first charge–discharge plateaus (Fig.4b) at 4.0–4.2 V are due to the removal of lithium ions from the other tetrahedral sites in which lithium ions do not have Li–Li interactions. The voltage differences ($\Delta\varphi_{p1}$ and $\Delta\varphi_{p2}$) of the $LiMn_{2-1.667x}Nb_xO_4$ ($x=0$, 0.01, 0.02, 0.03, and 0.04) electrodes between oxidation and reduction peaks are listed in Table 1. $\Delta\varphi_{p1}$ and $\Delta\varphi_{p2}$ are 228 and 201 mV for the $LiMn_2O_4$ electrode, obviously much larger than those for the Nb-doped electrodes, respectively. $LiMn_{1.95}Nb_{0.03}O_4$ sample shows the lowest potential interval between anodic and cathodic peak. The potential interval can be determined by the potential polarization of the active material during the charge and discharge process. Hence, the low potential interval demonstrates that the lithium insertion into the Nb-doped $LiMn_2O_4$ electrodes behave more likely as a Nernst system [26]. Based on the results mentioned above, it can be concluded that the improved reversibility and dynamic behaviors of $LiMn_2O_4$ can be attributed to the Nb doping.

Fig. 5 presents EIS profiles of $LiMn_{2-1.667x}Nb_xO_4$ ($x=0$, 0.01, 0.02, 0.03, and 0.04) and the corresponding equivalent circuit. EIS measurement performed at the open circuit voltage (about 3.0 V) after preliminary potentiostatic polarization at the same potential (3.0 V) for over 1 h in order to achieve an equilibrium condition, which is displayed in the form of Nyquist plot. According to the reported references [27,28], the symbols, R_s, R_f, R_{ct}, and W, represent the solution resistance, the diffusion resistance of Li^+ ions through SEI layer, the charge transfer resistance and Warburg impedance, respectively. The two constant phase elements (CPE1 and CPE2) associated with the interfacial resistance and charge transfer resistance [29]. According to the equivalent circuit, the charge transfer resistances of $LiMn_{2-1.667x}Nb_xO_4$ ($x=0$, 0.01, 0.02, 0.03, and 0.04) are calculated to be 2005, 968.7, 1314, 755.4 and 214.8 Ω, respectively. It can be found that the R_{ct} values vary greatly with different samples. Obviously, it can be concluded that Nb doping decreases the charge transfer resistance of $LiMn_2O_4$, indicating that the doping increases the conductivity. Similar positive results, such as Nb^{5+}-doped $LiMn_{1.5}Ni_{0.5}O_4$ [11] and $Li_3V_2(PO_4)_3$ [12] and $LiFePO_4$ [30], have also been proposed by other researchers. A decrease in charge transfer resistances may be due to that there is a possibility to increase the electronic conductivity of $LiMn_2O_4$ is to substitute multiply charged ions (i.e., M^{5+}) on a Mn^{3+} site, which should lead to an increase in electron concentration. The minimum R_{ct} value of Nb-doped $LiMn_2O_4$ means a lower electrochemical polarization, and this can lead to a better kinetic performance. In addition, we can also conclude that Nb-doped $LiMn_2O_4$ battery has lower cell impedance than that of $LiMn_2O_4$.

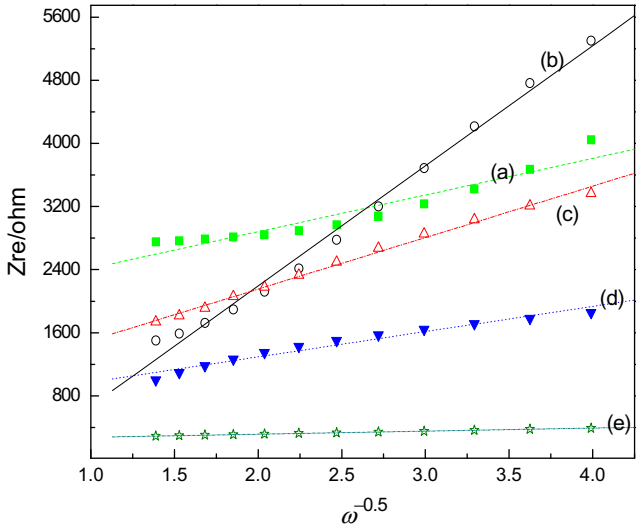

Fig. 6. Graph of Z_{re} plotted against $\omega^{-0.5}$ at low-frequency region for $LiMn_{2-1.667x}Nb_xO_4$ electrodes: (a) $x=0$, (b) $x=0.01$, (c) $x=0.02$, (d) $x=0.03$ and (e) $x=0.04$.

The diffusion coefficient (D_{Li}) of lithium ion can be calculated from the plots in the low-frequency region. The equation for the calculation of D_{Li} values by EIS can be expressed as [31]

$$Z_{re} = R_{ct} + R_s + \sigma\omega^{-1/2} \tag{3}$$

$$D_{Li} = \frac{R^2T^2}{2A^2n^4F^4C_{Li}^2\sigma^2} \tag{4}$$

where R is the gas constant, T the absolute temperature, A the surface area of the positive-electrode, n the number of electrons transferred in the half-reaction for the redox couple, F the Faraday constant, C_{Li} the concentration of lithium ion in solid, and σ is the Warburg factor, which is relative to $Z_{re}-\sigma$, which can be obtained from the slope of the lines in Fig. 6. The lithium diffusion coefficients of $LiMn_{2-1.667x}Nb_xO_4$ ($x=0$, 0.01, 0.02, 0.03, and 0.04) electrodes are calculated to be 1.24×10^{-16}, 0.115×10^{-16}, 0.626×10^{-16}, 2.61×10^{-16} and 181×10^{-16} $cm^2\,s^{-1}$, respectively. It is obvious that the lithium diffusion coefficients decrease and then increase due to the Nb doping. The diffusion coefficient of $LiMn_{1.933}Nb_{0.04}O_4$ is almost 146 times higher than that of $LiMn_2O_4$. This result clearly indicates that the lithium-ion mobility of $LiMn_2O_4$ can be effectively improved by Nb doping. Based on the above results and discussion, it can be found that Nb doping results in lower electrode polarization and a high lithium ion diffusion coefficient. Therefore, Nb doping can effectively improve the kinetic performance of $LiMn_2O_4$.

4. Conclusions

Powders of spinel Nb-doped $LiMn_2O_4$ were successfully synthesized at air conditions by a solid-state method. The phase transition reaction and electrochemical reaction process has not been changed by Nb doping, as indicated

by TG-DTA test and CV. All samples have the uniform, nearly cubic structure morphology with narrow size distribution, and the particle size of all prepared $LiMn_2O_4$ is about 1 μm. The low potential interval demonstrates that the lithium insertions into the Nb-doped $LiMn_2O_4$ electrodes behave more likely as a Nernst system, and the reversibility and dynamic behaviors are improved. The charge transfer resistance of Nb-doped $LiMn_2O_4$ electrode is lower than that of pure $LiMn_2O_4$. This suggests that Nb-doped $LiMn_2O_4$ battery has lower cell impedance than that of $LiMn_2O_4$.

Acknowledgments

This work was financially supported by the National Natural Science Foundation of China (Grant nos. 51274002 and 50902001), the China Postdoctoral Science Foundation (No. 2012M520749), and the Program for Innovative Research Team in Anhui University of Technology (No. TD201202).

References

[1] J. Yang, X.-y. Zhou, Y.-l. Zou, J.-j. Tang, A hierarchical porous carbon material for high power, lithium ion batteries, Electrochimica Acta 56 (2011) 8576–8581.
[2] Y. Wang, G. Cao, Developments in nanostructured cathode materials for high-performance lithium-ion batteries, Advanced Materials 20 (2008) 2251–2269.
[3] A. Manthiram, A. Murugan, A. Sarkar, T. Muraliganth, Nanostructured electrode materials for electrochemical energy storage and conversion, Energy and Environmental Science 1 (2008) 621–638.
[4] K. Matsuda, I. Taniguchi, Relationship between the electrochemical and particle properties of $LiMn_2O_4$ prepared by ultrasonic spray pyrolysis, Journal of Power Sources 132 (2004) 156–160.
[5] R. Santhanam, B. Rambabu, Research progress in high voltage spinel $LiNi_{0.5}Mn_{1.5}O_4$ material, Journal of Power Sources 195 (2010) 5442–5451.
[6] H.-C. Wang, C.H. Lu, Dissolution behavior of chromium-ion doped spinel lithium manganate at elevated temperatures, Journal of Power Sources 119–121 (2003) 738–742.
[7] R.S. Liu, C.H. Shen, Structural and electrochemical study of cobalt doped $LiMn_2O_4$ spinels, Solid State Ionics 157 (2003) 95–100.
[8] T. Kakuda, K. Uematsu, K. Toda, M. Sato, Electrochemical performance of Al-doped $LiMn_2O_4$ prepared by different methods in solid-state reaction, Journal of Power Sources 167 (2007) 499–503.
[9] C. Feng, H. Li, C. Zhang, Z. Guo, H. Wu, J. Tang, Synthesis and electrochemical properties of non-stoichiometric Li–Mn-spinel ($Li_{1.02}M_xMn_{1.95}O_{4-y}F_y$) for lithium ion battery application, Electrochimica Acta 61 (2012) 87–93.
[10] Y. Chen, K. Xie, Y. Pan, C. Zheng, Nano-sized $LiMn_2O_4$ spinel cathode materials exhibiting high rate discharge capability for lithium-ion batteries, Journal of Power Sources 196 (2011) 6493–6497.
[11] T.-F. Yi, Y. Xie, Y.-R. Zhu, R.-S. Zhu, M.-F. Ye, High rate micron-sized niobium-doped $LiMn_{1.5}Ni_{0.5}O_4$ as ultra high power positive-electrode material for lithium-ion batteries, Journal of Power Sources 211 (2012) 59–65.
[12] Y. Xia, W. Zhang, H. Huang, Y. Gan, C. Li, X. Tao, Synthesis and electrochemical properties of Nb-doped $Li_3V_2(PO_4)_3$/C cathode materials for lithium-ion batteries, Materials Science and Engineering: B 176 (2011) 633–639.
[13] B.J. Hwang, R. Santhanam, D.G. Liu, Characterization of nanoparticles of $LiMn_2O_4$ synthesized by citric acid sol–gel method, Journal of Power Sources 97–98 (2001) 443–446.
[14] S.-T. Myung, H.-T. Chung, Preparation and characterization of $LiMn_2O_4$ powders by the emulsion drying method, Journal of Power Sources 84 (1999) 32–38.
[15] M.Y. Song, I.H. Kwon, H.R. Park, D.R. Mumm, Electrochemical properties of $LiCo_yMn_{2-y}O_4$ synthesized using a combustion method in a voltage range of 3.5–5.0 V, Ceramics International 37 (2011) 2215–2220.
[16] C.H. Jiang, S.X. Dou, H.K. Liu, M. Ichihara, H.S. Zhou, Synthesis of spinel $LiMn_2O_4$ nanoparticles through one-step hydrothermal reaction, Journal of Power Sources 172 (2007) 410–415.
[17] Y.-P. Fu, C.-H. Lin, Y.-H. Su, J.-H. Jean, S.-H. Wu, Electrochemical properties of $LiMn_2O_4$ synthesized by the microwave-induced combustion method, Ceramics International 30 (2004) 1953–1959.
[18] Y.-R. Zhu, Y. Xie, R.-S. Zhu, J. Shu, L.-J. Jiang, H.-B. Qiao, T.-F. Yi, Kinetic study on $LiFePO_4$-positive electrode material of lithium-ion battery, Ionics 17 (2011) 437–441.
[19] L.A. Montoro, J.M. Rosolen, The role of structural and electronic alterations on the lithium diffusion in $Li_xCo_{0.5}Ni_{0.5}O_2$, Electrochimica Acta 49 (2004) 3243–3249.
[20] M. Kunduraci, G.G. Amatucci, The effect of particle size and morphology on the rate capability of 4.7 V $LiMn_{1.5+\delta}Ni_{0.5-\delta}O_4$ spinel lithium-ion battery cathodes, Electrochimica Acta 53 (2008) 4193–4199.
[21] X.-C. Tang, L.-X. Li, Q.-L. Lai, X.-W. Song, L.-H. Jiang, Investigation on diffusion behavior of Li^+ in $LiFePO_4$ by capacity intermittent titration technique (CITT), Electrochimica Acta 54 (2009) 2329–2334.
[22] K. Tang, X. Yu, J. Sun, H. Li, X. Huang, Kinetic analysis on $LiFePO_4$ thin films by CV, GITT, and EIS, Electrochimica Acta 56 (2011) 4869–4875.
[23] C.H. Chen, J. Liu, K. Amine, Symmetric cell approach and impedance spectroscopy of high power lithium-ion batteries, Journal of Power Sources 96 (2001) 321–328.
[24] H. Xia, S.B. Tang, L. Lu, Novel synthesis and electrochemical behavior of layered $LiNi_{0.5}Mn_{0.5}O_2$, Journal of Alloys and Compounds 449 (2008) 296–299.
[25] J.T. Son, H.G. Kim, New investigation of fluorine-substituted spinel $LiMn_2O_{4-x}F_x$ by using sol–gel process, Journal of Power Sources 147 (2005) 220–226.
[26] L. Xiao, Y. Zhao, Y. Yang, Y. Cao, X. Ai, H. Yang, Enhanced electrochemical stability of Al-doped $LiMn_2O_4$ synthesized by a polymer-pyrolysis method, Electrochimica Acta 54 (2008) 545–550.
[27] J. Liu, A. Manthiram, Understanding the improvement in the electrochemical properties of surface modified 5 V $LiMn_{1.42}Ni_{0.42}Co_{0.16}O_4$ spinel cathodes in lithium-ion cells, Chemistry of Materials 21 (2009) 1695–1707.
[28] A.Y. Shenouda, H.K. Liu, Electrochemical behaviour of tin borophosphate negative electrodes for energy storage systems, Journal of Power Sources 185 (2008) 1386–1391.
[29] X.-y. Zhou, J.-j. Tang, J. Yang, Y.-l. Zou, S.-c. Wang, J. Xie, L.-l. Ma, Effect of polypyrrole on improving electrochemical performance of silicon based anode materials, Electrochimica Acta 70 (2012) 296–303.
[30] D.G. Zhuang, X.B. Zhao, J. Xie, J. Tu, T.J. Zhu, G.S. Cao, One-step solid-state synthesis and electrochemical performance of Nb-doped $LiFePO_4$/C, Acta Physico-Chimica Sinica 22 (2006) 840–844.
[31] G.Q. Liu, H.T. Kuo, R.S. Liu, C.H. Shen, D.S. Shy, X.K. Xing, J.M. Chen, Study of electrochemical properties of coating ZrO_2 on $LiCoO_2$, Journal of Alloys and Compounds 496 (2010) 512–516.